Entrainment and Modulation of Turing Patterns under Spatiotemporal Forcing

Hiroto Shoji[1,2]

[1]*Kyoto Prefectural University of Medicine, Nishi-takatukasa 13, Kyoto 603-8334, Japan*
[2]*PRESTO, Japan Science and Technology Agency, 4-1-8, Honcho, Kawaguchi, Saitama 332-0012, Japan*
E-mail address: shoji@koto.kpu-m.ac.jp

(Received November 29, 2008; Accepted January 17, 2009)

We examine the time-evolutional behavior of self-organized Turing patterns under spatiotemporal forcing in one-dimensional systems. Based on the model equations, we apply a space-time-dependent external force. The entrainment and modulation of time-evolutional patterns are investigated numerically in one dimension. We develop a theoretical analysis to understand the obtained dynamics, and conjecture about the mode selection of the one-dimensional Turing pattern.

Key words: Reaction-diffusion System, Turing, External Forcing, Phase Equation

1. Introduction

Many biological systems display large-scale patterns that are much larger than their individual components. These self-organized patterns are observed in a broad range of systems and scales, from fish skin (Kondo and Asai, 1995) and animal coats (Murray, 2003) to the spatial distribution of individuals in ant colonies (Theraulaz *et al*., 2002). In many cases, patterns are formed through interactions among individuals within the systems.

Several groups have proposed possible candidates generating patterns. Turing (1952) offered what has been called "one of the most remarkable explanations of self-organized phenomena" by postulating a mechanism based on reacting and diffusing chemicals (Turing, 1952). This Turing mechanism is now called a diffusion-driven instability or Turing instability (Murray, 2003).

The effects of external forcing in pattern dynamics have also been studied. A typical problem is the synchronization of nonlinear oscillators with an externally applied periodic disturbance (Kuramoto, 1984). This is an example of nonlinear response in a nonequilibrium steady state. The effects of external forcing are interesting also because it might be useful to control the mesoscopic structures in material sciences. In fact, there are interesting experiments on pattern dynamics in nonequilibrium (Tabe and Yokoyama, 1995; Reigada *et al*., 2002).

The purpose of the present paper is to investigate, theoretically and by numerical simulation, the dynamics of Turing patterns under spatio-temporal external forcing. Epstein and coworker experimentally and numerically studied Turing-like patterns in chemical reactions under spatially periodic illumination (Horvath *et al*., 1999). Here we extend their study to spatio-temporal external forcing, carry out numerical simulations in one dimension, and develop a theoretical analysis to understand the results of the simulations.

The paper is organized as follows. In the next section, we start with a brief explanation of the FitzHugh-Nagumo equation and introduce external forcing. In Sec. 3, we present the entrained pattern to external forcing and the time-modulated pattern obtained numerically. The behavior is formalized in Sec. 4. Discussion is given in Sec. 5, including conjecture on mode selection of the Turing pattern.

2. FitzHugh-Nagumo Equation under External Forcing

The FitzHugh-Nagumo (FHN) equation is given by the coupled reaction diffusion equations (FitzHugh, 1961; Nagumo *et al*., 1962)

$$\partial u/\partial t = D_u \partial^2 u/\partial x^2 + u - u^3 - v, \tag{1}$$
$$\partial v/\partial t = D_v \partial^2 v/\partial x^2 + \gamma(u - \alpha v - \beta), \tag{2}$$

where the constants $\alpha, \beta, \gamma, D_u$, and D_v are all positive. This set of equations has been introduced as a model equation of impulse propagation along the nerve axon (Rinzel and Keller, 1973). In its original version, the diffusion term of the variable v was absent and only the u term existed in Eq. (2). By adding the diffusion term to the coefficient of D_v, the set of Eqs. (1) and (2) is that of the model equations for the Belousov-Zhabotinsky chemical reaction (Tyson and Keener, 1988).

Here we mention that Malevanets and Kapral (1997) considered a two-variable, site-specific reaction scheme where active sites can each accommodate a maximum of N molecule maximum for species U and a separate N molecule maxium for species V. The vacancies corresponding to these species will be denoted U^* and V^*, respectively. The mechanism comprised the following processes:

$$\begin{array}{lcr} 2U + U^* \xrightarrow{k_1} 3U,\; 2U^* + U \xrightarrow{k_1^*} 3U^*, & U^* + V & \xrightarrow{k_2} U + V \\ & k_3 \uparrow & \downarrow k_3^* \\ & U^* + V^* & \xrightarrow{k_2} U + V^*. \end{array}$$

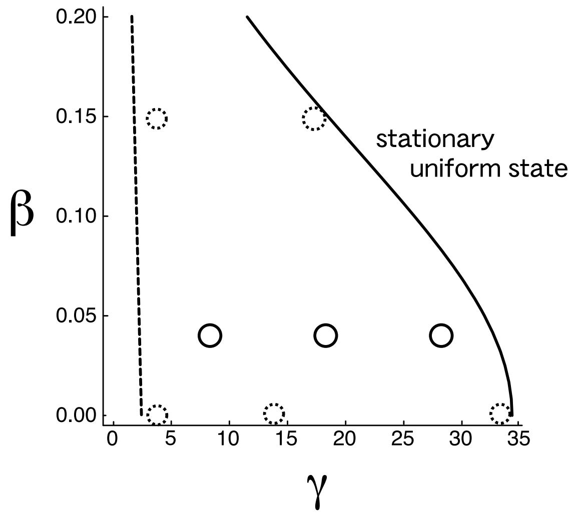

Fig. 1. Bifurcation diagram for $D_u = 0.15$, $D_v = 15.0$, and $\alpha = 0.5$ in Eqs. (1) and (2). The thick full line and dotted line are the Turing bifurcation and the Hopf bifurcation, respectively. The full and dotted circles indicate the parameters we use in Fig. 3 and in our comparison of (γ, β) in the Discussion section.

If the rate constants satisfy $k_2 = k_2^*$ and $k_3 = k_3^*$, and with the diffusion term considering the Brownian motions of molecules, the dimensionless reaction diffusion system can be turned to yield a desired valued of FHN equations (1) and (2) (Malevanets and Kapral, 1997).

Equations (1) and (2) each have a time-independent uniform solution $(\bar{u}, \bar{v})$ which are defined through $\bar{u}-\bar{u}^3-\bar{v} = 0$ and $\bar{u} - \alpha\bar{v} - \beta = 0$. We are concerned with the monostable situation when the diffusions are absent. The linear stability analysis of the uniform solution is readily carried out. Put $(u - \bar{u}, v - \bar{v}) \sim \exp(ikx + \lambda t)$. The eigenvalue is a solution of the algebraic equation

$$\lambda^2 + \{(D_u + D_v)k^2 + (3\bar{u}^2 + \alpha\gamma - 1)\}\lambda + (D_u k^2 + 3\bar{u}^2 - 1)(D_v k^2 + \alpha\gamma) + \gamma = 0. \quad (3)$$

The uniform solution $(\bar{u}, \bar{v})$ becomes unstable when the real part of λ is positive. Actually, we consider a situation where the eigenvalue is always real. The eigenvalue becomes positive first at the critical wave number given by $k_c^2 = (1-3\bar{u}^2)/2D_u - \alpha\gamma 2D_v$. The parameter region where $(\bar{u}, \bar{v})$ is linearly unstable is given by the condition

$$\frac{\{D_v(1-3\bar{u}^2) - \alpha\gamma D_u\}^2}{4D_u D_v} + \alpha\gamma(1-3\bar{u}^2) - \gamma > 0. \quad (4)$$

It is readily shown that the condition $k_c > 0$ is satisfied if $D_u << D_v$. Especially, Hopf instability occurs for

$$3\bar{u}^2 + \alpha\gamma - 1 < 0. \quad (5)$$

Figure 1 displays the bifurcation thresholds for $D_u = 0.15$, $D_v = 15.0$, and $\alpha = 0.5$ in Eqs. (1) and (2). The full line is the Turing bifurcation given by (4), whereas the dotted line is the Hopf bifurcation line given by (5). On the right side of the full line, the uniform time-independent solution is linear stable. We have carried out numerical simulations for $D_u = 0.15$, $D_v = 15.0$, and $\alpha = 0.5$ with changes in parameter β and γ in which Turing instability occurs.

In order to investigate post-threshold behavior, we have carried out numerical simulations of Eqs. (1) and (2) in one dimension. The calculation scheme is applied to the fully implicit finite difference method with the system size $L = 80\pi$ divided into 4096 grids ($\delta x = 80\pi/4096$) and with periodic boundary condition. The chosen time increment is $\delta t = 0.01$. The unstable uniform solution $(\bar{u}, \bar{v})$ with a small random perturbation is used as the initial condition, providing ten different random perturbations for each value of γ.

Now we consider a case where the system is exposed through periodically arrayed slits by illuminating light and the slit moves at constant velocity Ω/q_f with $2\pi/q_f$ period of the slits. As a result, we assume that the autocatalysis rate of U and U^* is the affected rate Γ where Γ represents the effect of illumination traveling to the right at the velocity Ω/q_f, and Γ is the sinusoidal force providing a sufficiently small forcing ϵ. In this way, the set of Eq. (1) has an additive term $\Gamma(x, t) = \epsilon\cos(q_f x - \Omega t)$. The set of equations that we study becomes

$$\partial u/\partial t = D_u \partial^2 u/\partial x^2 + u - u^3 - v + \epsilon\cos(q_f x - \Omega t), \quad (6)$$

$$\partial v/\partial t = D_v \partial^2 v/\partial x^2 + \gamma(u - \alpha v - \beta). \quad (7)$$

The parameters are fixed as $D_u = 0.15$, $D_v = 15.0$, $\alpha = 0.5$, and $\beta = 0.04$ as in the previous line, whereas γ, ϵ, and q_f are varied in numerical simulations. In this paper, we consider only a case where the external forcing is applied at the beginning of each simulation. The wave numbers of the obtained patterns are the same as the wave number of the external forcing, to the extent that the intrinsic wave number of a system is not much different from external forcing, Fig. 4(c) shows.

When the external force is small enough ($\epsilon << 1$), the Turing pattern is not affected appreciably. However, when the magnitude of the external forcing exceeds a certain threshold, the pattern undergoes an induced motion. Figure 2(b) shows the concentration variation when the pattern is entrained by the external forcing. We have repeated the simulation by changing (q_f, ϵ) and have obtained the phase diagram shown in Fig. 3. When the strength of the forcing is strong enough in the region indicated by $\times$, the periodic pattern is entrained completely by the external forcing, as shown in Fig. 4(a), where the periodic domains travel with the external velocity Ω/q_f. When ϵ is small in the region indicated by $\square$, the domains do not exhibit a smooth traveling motion but undergo a periodic modulation. This can be seen in Fig. 4(b).

3. Theoretical Analysis

Now we formulate the modes in the case of the model equation. Numerical simulation shows that Eqs. (1) and (2) have motionless periodic solutions, and we write

$$u = \bar{u} + u_1\cos(qx), \quad v = \bar{v} + v_1\cos(qx).$$

Substituting these into (1) and (2) and ignoring the higher harmonics generated by the nonlinear term, we obtain the

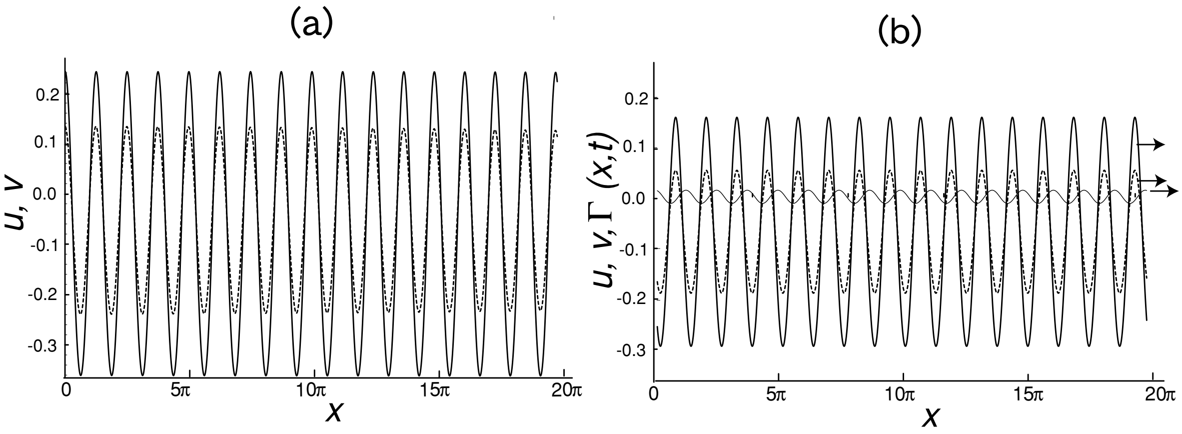

Fig. 2. Spatial variations of $u(x, t)$ (thick dotted line) and $v(x, t)$ (thick full line), which are (a) statical as obtained numerically from Eqs. (1) and (2) for $D_u = 0.15$, $D_v = 15.0$, $\alpha = 0.5$, $\beta = 0.04$, and $\gamma = 28.0$; and (b), which are traveling to the right as indicated by the arrow obtained numerically from (6) and (7) for the same with $q_f = 1.600$, $\Omega = 0.05$, and $\epsilon = 0.01270$. The thin full line indicates $\Gamma = \epsilon\cos(q_f x - \Omega t)$. Although the system size is 80π, only the interval between 0 and 20π is displayed, for the sake of clarity.

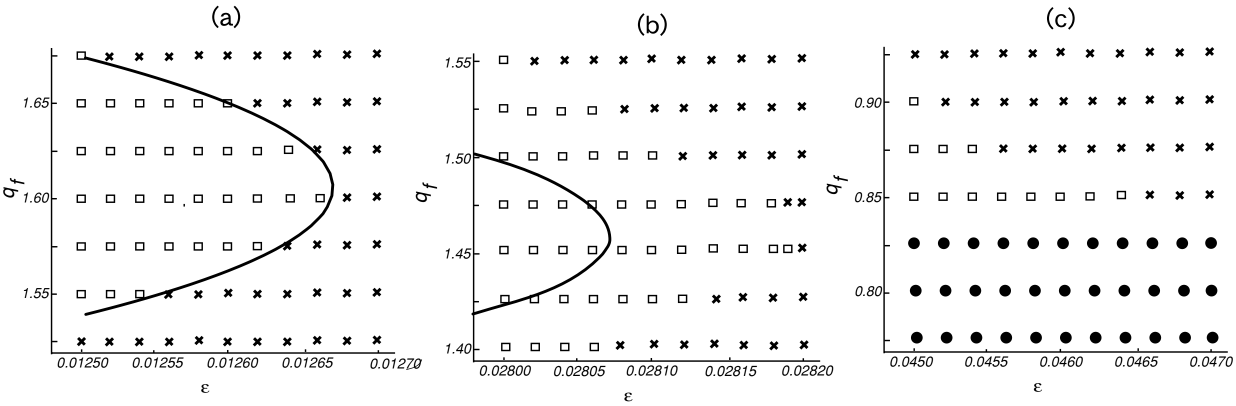

Fig. 3. Behavior in the $q_f - \epsilon$ plane by solving (6) and (7) numerically for (a) $\gamma = 28.0$, (b) $\gamma = 18.0$, or (c) $\gamma = 8.0$. The other parameters are for $D_u = 0.15$, $D_v = 15.0$, $\alpha = 0.5$, and $\beta = 0.04$. When the strength of the forcing is strong enough in the region indicated by $\times$, the periodic pattern entrained completely by external forcing as shown in Fig. 4(a), where the periodic domains travel with the external velocity Ω/q_f. When ϵ is small in the region indicated by $\Box$, the domains do not undergo an induced traveling but exhibit a periodic modulation. This can be seen in Fig. 4(b). When q_f is beyond the threshold wave number in the region indicated by $\bullet$, each mode splits into two. This can be seen in Fig. 4(c). The thick line is drawn by Eq. (15).

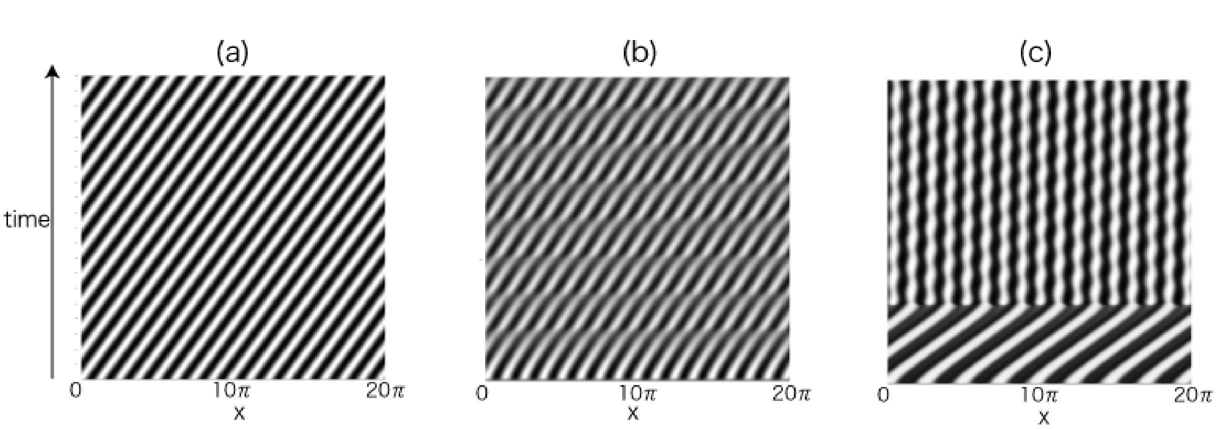

Fig. 4. Space (horizontal) $-$ time (vertical) plot of $u(x, t)$ for $q_f = 1.625$, $\gamma = 28.0$ and (a) $\epsilon = 0.01266$, (b) $\epsilon = 0.01260$, whereas (c) $q_f = 0.825$, $\gamma = 8.0$, and $\epsilon = 0.0466$. The other parameters are $D_u = 0.15$, $D_v = 15.0$, $\alpha = 0.5$, and $\beta = 0.04$ in Eqs. (6) and (7). The value of u is larger (smaller) for lighter (darker) regions. No modulation appears in (a). The modulation occurs periodically in time but uniformly in space in (b). The wave number of the external forcing is beyond the ranges of intrinsic wave number in Eqs. (6) and (7) in (c).

set of equations for u_1 and v_1

$$\begin{aligned}&(-D_u q^2 + 1)u_1 - v_1 - \tfrac{3}{4}u_1^3 - 3\bar{u}^2 u_1 = 0,\\&\gamma u_1 - (D_v q^2 + \alpha\gamma)v_1 = 0.\end{aligned} \tag{8}$$

When the magnitude of external force is increased, the motionless solution (7) becomes unstable, as shown in Figs. 3 and 4. Modulation and entrained solutions appear after destabilization of the motionless distribution in Fig. 3. Now we consider that the modulation solution can be approximated by

$$u = \bar{u} + u_1(1 + \phi_1(t))\cos(q_f x - \Omega t + \theta(t)), \tag{9}$$

$$v = \bar{v} + v_1(1 + \phi_2(t))\cos(q_f x - \Omega t + \theta(t)), \tag{10}$$

where the time-evolution equation for the terms ϕ_1 and ϕ_2 relating to the amplitudes and that for the phase $\theta(t)$ are to be derived. Substituting (9) and (10) into (6) and (7), multiplying each equation by $\cos(q_f x - \Omega t + \theta(t))$ and carrying out the integral over one spatial period, we obtain

$$\begin{aligned}u_1\frac{\partial\phi_1}{\partial t} &= \left(u_1 - D_u q_f^2 u_1 - \frac{9}{4}u_1^3 - 3u_1\bar{u}^2\right)\phi_1(t)\\&\quad - v_1\phi_2(t) + \epsilon\cos\theta(t),\end{aligned} \tag{11}$$

$$v_1\frac{\partial\phi_2}{\partial t} = \gamma u_1\phi_1(t) - (D_v q_f^2 v_1 + \alpha\gamma v_1)\phi_2(t). \tag{12}$$

Similarly, multiplying (9) by $\sin(q_f x - \Omega t + \theta(t))$, and carrying out the integral over one spatial period, we obtain the equation for the phase $\theta(t)$

$$u_1(1 + \theta(t))\left(\Omega - \frac{\partial\theta}{\partial t}\right) = \epsilon\sin\theta(t). \tag{13}$$

$\phi_1(t)$ and $\phi_2(t)$, which evolve slowly in time, are eliminated adiabatically. Putting $d\phi_1/dt = d\phi_2/dt = 0$, we obtained the time-evolution equation for phase $\theta(t)$

$$\frac{\partial\theta}{\partial t} = \Omega + \epsilon'\sin(\theta(t) + \xi), \tag{14}$$

where $\epsilon' = \epsilon(\Omega^2/H^2 + 1/u_1^2)^{1/2}$, $\tan\xi = -(\Omega/H)u_1$, and $H = (1 - D_u q_f^2)u_1 - 3u_1\bar{u}^2 - (9/4)u_1^3 - (\gamma u_1/q_f^2 D_v v_1 + \alpha\gamma v_1)v_1$. Equation (14) implies that when $\Omega < \epsilon'$, there is a stable equilibrium solution that corresponds to the complete entrainment with the external force. When $\Omega > \epsilon'$, this entrainment breaks down. $\Omega = \epsilon'$ is the theoretically obtained stability limit of the modulated traveling wave, that has the same velocity as the external force. As shown in Eq. (8), u_1 and v_1 can be expressed as functions of q_f. In general, the stability limit can be written as

$$\epsilon = \Omega\Big/\left(\frac{\Omega^2}{H^2} + \frac{1}{u_1^2}\right)^{1/2}. \tag{15}$$

We investigate the wave number indicated by the regions between the full and dotted lines in Fig. 1. We fix the parameters as $D_u = 0.15$, $D_v = 15.0$, and $\alpha = 0.5$; the remaining parameters γ, β are varied. We use the set of parameters (γ, β) indicated in Fig. 1 as solid and dotted circles. Figure 3 shows the result of changing γ on $\beta = 0.04$. In order of increasing γ, accordance between numerical simulation and theoretical analysis is not seen. Moreover, this marked tendency rises significantly according to the $|\beta|$ (data not shown). In $\beta = 0.00$, good agreement can be seen for a wide range of $\gamma(14.0 < \gamma < 34.0)$, whereas in the case of $\beta = 0.15$, the parameter range, which shows good agreement, is only near the Turing bifurcation point.

4. Discussion

We have studied the dynamics of Turing patterns under conditions of spatio-temporal forcing. In the present investigation, we successfully predicted the phase transition point between the modulations and entrainment, and found that this point agrees well with the simulations (see Fig. 3(a)). Moreover, we examined the parameters indicated by the dotted circles in Fig. 1 (data not shown).

The model system without an external forcing is Turing one in which self-organized and static pattern appears. Therefore in Eqs. (6) and (7) the obtained patterns (modulation or entrainment) might be considered as the results after competition between Turing's static property and entrainment one of external force. Moreover, Figs. 3(a) and (b) shows there is one mode which need maximum strength of external force.

Finally, we discussed mode selection in the Turing patterns. In pattern formation phenomena, a fundamental unsolved problem in nonvariational disspative systems is to determine the general principle of mode selection beyond a bifurcation threshold. Here we assume the wavenumber which most commonly appears can tolerate with the largest external forcing. In this respect, it would be interesting to explore the possibility that some resonance condition might be related to the mode selection. That is, a periodic pattern might respond most strongly to an external periodic modulation whose period is the same as that of the intrinsic spatial period. To examine this possibility, we have carried out numerical simulations of Turing patterns without external forcing. For example, we obtained the intrinsic wave number $1.575 \le q \le 1.625$ at $\beta = 0.04$ and $\gamma = 28.0$, changing the initial distribution sets ten times. It is found from Fig. 3(a) that these wave number coincides with the last wave number q_f where the time-periodic modulation becomes unstable by increasing ϵ and the complete entrainment with the external force starts. We have also carried out numerical simulations for $\gamma = 34.0, \beta = 0.00$ and $\gamma = 14.0, \gamma = 0.00$ and found that the intrinsic wave numbers of q_f show good agreement with the last wave number of q_f. We emphasize that this property is not limited near the Turing bifurcation point. This numerical evidence strongly supports our conjecture. We shall return to this problem in further detail in the near future.

Acknowledgments. We are grateful to Professor Takao Ohta, Kyoto University, and to Dr. Hidekazu Tokuda, Kyoto University, for their help. We also thank H. Nagayama and Y. Tonosaki for their helpful comments.

References

FitzHugh, R. (1961) Impulses and physiological states in theoretical models of nerve membrane, *Biophys. J.*, **1**, 445–466.

Horvath, A. K., Dolnik, A. K., Munuzuri, A. P., Zhabotinsky, A. M. and Epstein, I. R. (1999) Control of Turing structures by periodic ilumination, *Phys. Rev. Lett.*, **83**, 2950–2953.

Kondo, S. and Asai, R. (1995) A viable reaction-diffusion wave on the skin of *Pomacanthus*, a marine angelfish, *Nature*, **376**, 765–768.

Kuramoto, Y. (1984) *Chemical Oscillations, Waves and Turblance*, Springer-Verlag, New York.

Malevanets, A. and Kapral, R. (1997) Microscopic model FitzHugh-Nagumo dynamics, *Phys. Rev. E*, **55**, 5657–5681.

Murray, J. D. (2003) *Mathematical Biology*, 3rd ed., Springer-Verlag, Berlin.

Nagumo, J., Arimoto, S. and Yoshikawa, Y. (1962) An active pulse transmission line simulating nerve axon, *Proc. IRE*, **50**, 2061–2071.

Reigada, R., Sugues, F. and Mikhailov, M. A. (2002) Traveling waves and nonequilibrium stationary patterns in Two-component reactive langmuir monolayers, *Phys. Rev. Lett.*, **89**, 038301–038305.

Rinzel, J. and Keller, J. B. (1973) Traveling wave solutions of a nerve conduction equation, *Biophys. J.*, **13**, 1313–1337.

Tabe, Y. and Yokoyama, H. (1995) Two-dimensional dynamic patterns in illuminated langmuir monolayers, *Langmuir*, **11**, 4609–4613.

Theraulaz, G. *et al*. (2002) Spatial patterns in ant colonies, *PNAS*, **99**, 9645–9649.

Turing, A. (1952) The chemical basis of morphogenesis, *Phil. Trans. R. Soc. Lond.*, **B237**, 37–72.

Tyson, J. J. and Keener, J. P. (1988) Singular perturbation theory of traveling waves in excitable media, *Physica*, **D32**, 327–361.